

Journal Pre-proof

S1PR2 inhibitors potently reverse 5-FU resistance by downregulating DPD expression in colorectal cancer

Yu-Hang Zhang, Dong-Dong Luo, Sheng-Biao Wan, Xian-Jun Qu



PII: S1043-6618(19)32493-4
DOI: <https://doi.org/10.1016/j.phrs.2020.104717>
Reference: YPHRS 104717

To appear in: *Pharmacological Research*

Received Date: 6 November 2019
Revised Date: 6 February 2020
Accepted Date: 17 February 2020

Please cite this article as: Zhang Y-Hang, Luo D-Dong, Wan S-Biao, Qu X-Jun, S1PR2 inhibitors potently reverse 5-FU resistance by downregulating DPD expression in colorectal cancer, *Pharmacological Research* (2020), doi: <https://doi.org/10.1016/j.phrs.2020.104717>

This is a PDF file of an article that has undergone enhancements after acceptance, such as the addition of a cover page and metadata, and formatting for readability, but it is not yet the definitive version of record. This version will undergo additional copyediting, typesetting and review before it is published in its final form, but we are providing this version to give early visibility of the article. Please note that, during the production process, errors may be discovered which could affect the content, and all legal disclaimers that apply to the journal pertain.

© 2020 Published by Elsevier.

**S1PR2 inhibitors potently reverse 5-FU resistance by downregulating DPD
expression in colorectal cancer**

Running title: S1PR2 inhibitors prevent 5-FU resistance by downregulating DPD

Yu-Hang Zhang^{1†}, Dong-Dong Luo^{2†}, Sheng-Biao Wan^{2*}, Xian-Jun Qu^{1*}

¹Department of Pharmacology, School of Basic Medical Sciences, Capital Medical University, Beijing, China, 100069

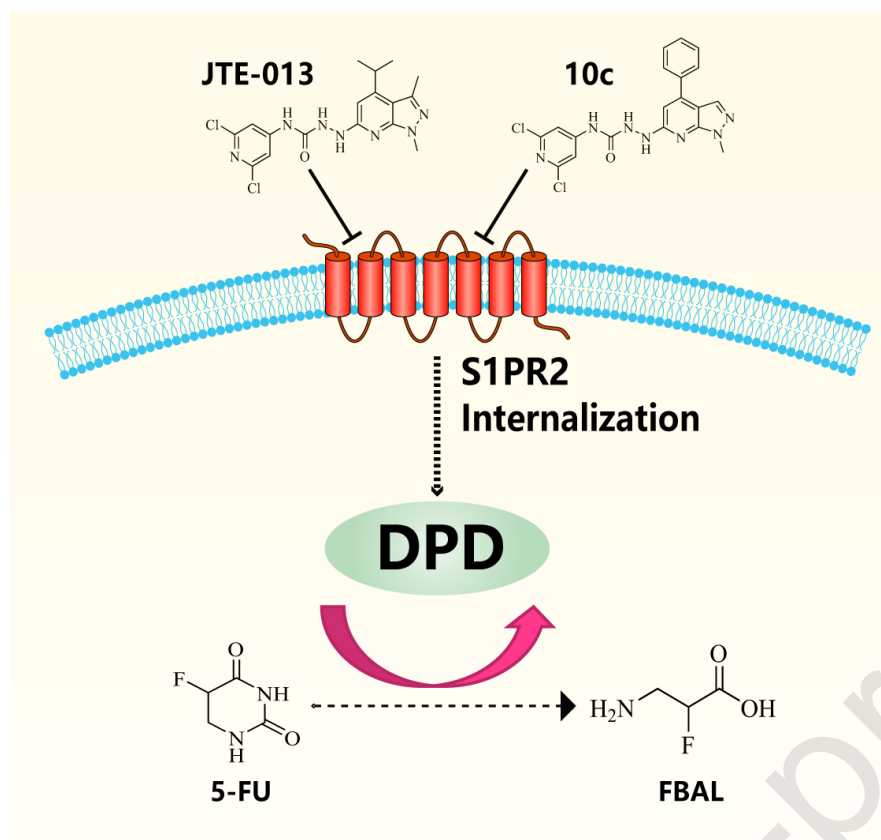
²Laboratory for Marine Drugs and Bioproducts of Qingdao National Laboratory for Marine Science and Technology, Key Laboratory of Marine Drugs, Ministry of Education, School of Medicine and Pharmacy, Ocean University of China, Qingdao, China, 266003

[†]These authors contributed equally: Yu-Hang Zhang, Dong-Dong Luo

*Corresponding authors: Sheng-Biao Wan and Xian-Jun Qu

Tel/Fax: 86-010-83911516, e-mail: quxj@ccmu.edu.cn or biaowan@ouc.edu.cn

Graphical abstract



Highlights

- S1PR2 is the potential upstream regulator of DPD expression in CRC cells
- JTE-013 effectively reversed 5-FU resistance of CRC both *in vivo* and *in vitro*
- JTE-013 levels off DPD-catalyzed degradation of intracellular 5-FU in CRC

Abstract

In this study, S1PR2 was reckoned as a brand-new GPCR target for designing inhibitors to reverse 5-FU resistance. Herein a series of pyrrolidine pyrazoles as the S1PR2 inhibitors were designed, synthesized and evaluated for their activities of anti-

FU-resistance. Among them, the most promising compound JTE-013, exhibited excellent inhibition on DPD expression and potent anti-FU-resistance activity in various human cancer cell lines, along with the *in vivo* HCT116^{DPD} cells xenograft model, in which the inhibition rate of 5-FU was greatly increased from 13.01% to 75.87%. The underlying mechanism was uncovered that JTE-013 demonstrated an anti-FU-resistance activity by blocking S1PR2 internalization to the endoplasmic reticulum (ER), which inhibited the degradation of 5-FU into α -fluoro- β -alanine (FBAL) by downregulating tumoral DPD expression. Overall, JTE-013 could serve as the lead compound for the discovery of new anti-FU-resistance drugs.

Significance: This study provides novel insights that S1PR2 inhibitors could sensitize 5-FU therapy in colorectal cancer.

Key words: Colorectal cancer (CRC); S1P receptor 2 (S1PR2); Dihydropyrimidine dehydrogenase (DPD); 5-FU resistance.

Introduction

5-Fluorouracil (5-FU) has long been the basic drug for colorectal cancers (CRCs), however, drug resistance remains the great obstacle to its clinical use [1, 2]. In mammalian cells, 5-FU is converted into fluorodeoxyuridine monophosphate

(FdUMP), which forms a stable complex with thymidylate synthase (TS or TYMS) and causes cytotoxicity by inhibiting TS activity [3, 4]. Dihydropyrimidine dehydrogenase (DPD or DPYD)-mediated conversion from 5-FU to dihydrofluorouracil (DHFU) is a rate-limiting step of 5-FU catabolism [5, 6]. Therefore, high levels of TS and DPD are widely taken as two major causes of 5-FU resistance [7]. Currently, many reports have been issued about the modulatory mechanisms of TS expression, yet the knowledge of DPD is still limited to its single nucleotide polymorphisms (SNPs). Nonetheless, known SNPs only account for approximately 30% cases of severe resistance to 5-FU [8, 9] and the majority of patients who developed 5-FU resistance do not carry known toxicity-associated SNPs for *DPYD* [10]. Most importantly, 5-FU itself is the ideal inhibitor of TS and leucovorin is used to stabilize FdUMP-TS complex [11, 12], whereas current DPD inhibitors (i.e. CDHP in S-1 regimen) suppress catalytic activity of DPD only in liver but not in cancer cells [13, 14]. Moreover, it was reported that these reversible competitive enzyme inhibitors of DPD augmented the liver toxicity of 5-FU [15]. Therefore, it is of paramount importance to elucidate the regulatory target of tumoral DPD for the sake of optimizing 5-FU regimens.

Even though it was reported that increased H3K27me3 at the *DPYD* promoter could downregulate DPD expression [16], it was still difficult for an inhibitor to directly enter into the nucleus and modify the methylation of H3K27 in cancer cells. If a transmembrane receptor could be identified as the upstream regulator of

H3K27me3, the inhibitors of this transmembrane receptor would effectively downregulate the expression of DPD in cancer cells. S1PR2, one of five G protein-coupled receptors (GPCRs) of sphingosine-1-phosphate (S1P), has been ignored in the development of drug discovery [17]. The immunomodulatory drug fingolimod (FTY720, Gilenya^R) was approved for treatment of relapsing-remitting multiple sclerosis, due to its impressive efficacy and good tolerability [18-20]. As fingolimod resembles in chemical structure of sphingosine, it serves as the phosphorylated substrate of sphingosine kinase 2 (SphK2) [21, 22]. The metabolite fingolimod-P showed similar affinity as S1P by binding with S1PR1, S1PR3, S1PR4 and S1PR5 [23, 24]. However, it was verified that Fingolimod-P is not a ligand for S1PR2 [25]. Several inhibitors of S1PR_{1,3-5}, such as Ponesimod and Etrasimod, have currently entered into the stage III clinical trials [26, 27]. However, S1PR2 is still left as the vacant GPCR target for further investigation.

In this study, we found that S1PR2 inhibitors could downregulate DPD expression to suppress the degradation of intracellular 5-FU into inactive α -fluoro- β -alanine (FBAL). A series of novel pyrrolidine pyrazole inhibitors referenced to JTE-013 were synthesized and evaluated for their activity of overcoming 5-FU resistance through downregulating tumoral DPD. We thus suggest that JTE-013, the most superior S1PR2 inhibitor, could be developed as a potential reversal agent of 5-FU resistance for clinical applications.

Results

Identification of S1PR2 as a potential upstream regulator of DPYD expression in

TCGA database and cell lines. To investigate the potential role of S1PR2 in regulating 5-FU resistance, we firstly screened the expression data from The Cancer Genome Atlas (TCGA). Overall, S1PR2 expression was significantly increased in a variety of tumoral samples as compared to the paracancerous tissues, including colorectal cancer, skin cutaneous melanoma and brain lower grade Glioma (Fig. 1A and 1B). Among these cancer types, CRC was the only cancer type given 5-FU-based adjuvant chemotherapy as the first-line treatment. Since DPD (encoded by DPYD or dpyd), TS (encoded by TYMS) and thymidine phosphorylase (encoded by TYMP) are all considered to be involved in the development of 5-FU resistance, we further screened TCGA database to identify which gene might be upregulated by S1PR2^{high}. DPYD expression showed positive correlation with S1PR2 in CRCs ($R = 0.75$) but not in paracancerous tissues ($R = 0.31$). Neither TYMS nor TYMP were significantly correlated to S1PR2 in CRCs or paracancerous tissues (Fig. 1C and D).

Further, we determined the expressions of S1PR2 and DPD in various naïve cell lines, including HCT116, HT-29, SW620, LOVO, NCM460, MCF-7, BT474, Hela, Huh7 and ccHEL-1 cells. It showed a significant difference in the expressions of S1PR2 and DPD among these cell lines but a satisfying consistence between high S1PR2 and elevated DPD. HCT116, SW620, Huh7 and ccHEL-1 cells were found with both higher S1PR2 and elevated DPD as compared with other cell lines (Fig.

1E). We further performed the RT-qPCR assay to analyze the mRNA levels of *s1pr2* and *dpd*. Higher levels of *s1pr2* and *dpd* were also seen in HCT116, SW620, Huh7 and cccHEL-1 cells than other cell lines (Fig. 1F). Also, S1PR2 shRNA was transfected into HCT116, SW620, Huh7 and cccHEL-1 cells to determine their DPD levels. It showed that these four cell lines transfected with S1PR2 shRNA all exhibited lower DPD expression as compared with their vector controls (Fig. 1G). Finally, we treated the above shS1PR2 cells with dose gradient of 5-FU with the concentrations from 6.25 to 100 μ M. It showed that S1PR2 shRNA significantly increased the sensitivity of 5-FU treatment in HCT116, SW620, Huh7 cells but not in cccHEL-1 cells (Fig. 1H). Overall, these results suggest that S1PR2 might be a novel GPCR target for designing reversal agents of 5-FU resistance by downregulating DPD expression.

Synthetic chemistry of S1PR2 inhibitors. Since shS1PR2 could effectively enhance the sensitivity of cancer cells to 5-FU treatment by downregulating DPD expression, we sought to design, synthesize and evaluate a series of compounds referenced to JTE-013. The syntheses of S1PR2 inhibitors were performed as shown in Scheme 1. All S1PR2 inhibitors were synthesized from hydrazine intermediates (**6a-6c**, **13a-13k** or **22**) by condensation with the corresponding acid azide. The reflux of 5-amino-1,3-dimethylpyrazole in acetic acid with esters afforded the correspondent compounds **4a-4c**. The reaction yield was low and the separation of the product was difficult through

silica gel chromatography due to the acylated side product from the reaction of 5-amino-1,3-dimethylpyrazole with solvent acetic acid with close polarity as the product. Fortunately, ethyl acetate allowed the separation of the product from the acylated side product. Compounds **5a-5c** afforded from bromination of **4a-4c**, followed by reaction with 80% hydrazine hydrate in ethanol to produce the key intermediates **6a-6c**. The 2,6-dichloropyridine moiety **8** was derived from the commercially available 2,6-dichloroisonicotinic acid **7** in straightforward steps. Reflux of compound **8** in toluene produced the isocyanate **9**. Compounds **10a-10c** were obtained through subsequent adding of the solutions of hydrazine **6a-6c** in tetrahydrofuran (THF). Iodination of compound **4a** to produce compound **11**, and the replacements of iodine atom by different substitutions were carried out through Suzuki coupling reaction to obtain **12a-12k**. Subsequently, the same procedures were performed to produce **14a-14k**. The different substituted isonicotinic acid **15a-15d** were used to gain acid azide **16a-16d** and subsequent combination with **6a** to obtain **18a-18d**. Starting from 2,4-dichloro-7*H*-pyrrolo[2,3-*d*] pyrimidine **19**, compound **21** was obtained through substitution and methylation. Compound **23** was then prepared following a similar two-step sequence as shown in Scheme 1 (for more details, please see the Supplementary Methods).

SAR of S1PR2 inhibition. *In vitro* anti-5-FU resistance activities against human colorectal cell lines, including HCT116, HT-29 and NCM460, were analyzed by 3-

(4,5-dimethylthiazol-2-yl)-2,5-diphenyltetrazolium bromide (MTT) assay. The inhibition rates of these compounds at the concentrations of 6.25, 12.5, 25, 50, 100, 200 μM and the IC_{50} values were listed in Table 1 (left panel). All these compounds were then combined with 10 μM 5-FU for further analysis of the EC_{50} values. The results were listed in Table 1 (right panel). JTE-013, the reported S1PR2 inhibitor, was resynthesized and identified as a hit compound with the EC_{50} of 18.28 μM in HCT116 cells. The design of inhibitors could not be aided by crystallographic methods because crystal structure of S1PR2 has still not been elucidated. Therefore, the SAR of S1PR2 inhibition is mainly illuminated by introducing various modifications to different regions of the hit molecule.

SAR exploration initiated with the investigation of various substitutions at the pyrrolopyridine structure of S1PR2 inhibitors (Table 1). Methyl and cyclopropyl substitutions on the pyridine ring show no improvement (**10a** and **10b** vs **JTE-013**), whereas phenyl substitution exhibits better S1PR2 potencies (**10c** vs **JTE-013**). These results indicate that the inhibitory effect of the compounds on S1PR2 is enhanced by the increase of volume of the hydrophobic group. Replacements of hydrogen on pyrrole ring of **10a** with bulk group are also beneficial (**14a-14k**), in particular, as are pyridine (**14a**) and fluorine benzene (**14d**). The effect of the chloric substitutions at 2,6-dichloropyridine structure on JTE-013 was subsequently investigated. The mono-substituted pyridines showed no improvement (**18a-18d** vs **JTE-013**), whereas non-substituted pyridine is a weaker inhibitor than the substituted pyridines. The above

results demonstrate that moderate bis-substitutions are more suitable. The impact of pyrrolopyridine structure was subsequently examined and replacements of pyrrolopyridine moiety on hit **1** with pyrrolopyrimidine are not beneficial (**23** vs **JTE-013**). In conclusion, the data of SAR illustrate that the attachment of alkyl or aryl groups to the fused ring greatly improves S1PR2 potency and the inhibitory effect is further enhanced by the addition of size of hydrophobic group.

According to the EC₅₀ and IC₅₀ values, we subsequently selected 5 most potent and selective S1PR2 inhibitors to analyze their activity of inhibiting DPD expressions by western blotting assay. It showed that compounds **10c** and **JTE-013** demonstrated strong activity in preventing the expression of DPD (Fig. 2A). Moreover, we previously ascertained that 5-FU could induce S1PR2 to internalize to the ER. Herein, we found that compounds **10c** and **JTE-013** effectively restrained the 5-FU-induced S1PR2 internalization (Fig. 2B). Enlightened from our previous study, we further validated the ER stress signaling under the dose gradient of JTE-013 with the concentrations from 1.3 to 100 μM. The reported JMJD3-H3K27me3-DPD pathway was also determined to be gradually suppressed when cancer cells were treated with higher dose of JTE-013 (Fig. S1). These *in vitro* results suggest that compounds **10c** and **JTE-013** could be developed as the potential 5-FU resistance inhibitors through the mechanism of preventing tumoral DPD.

Binding models for compounds 10c and JTE-013 in the S1PR2-binding pocket.

To explore the interaction between receptor residues and ligands, a homology model of S1PR2 was established and the binding site was deduced based on the known crystal complex of S1PR1 and ligand (Fig. 3A). Compounds **10c** and **JTE-013** (Fig. 3B) were well docked into the ligand-binding cavity. Comparing the binding modes of compound **10c** to **JTE-013** (Fig. 3C and D), both **10c** and **JTE-013** adopt a similar “U-shape” conformation. For **JTE-013**, however, five hydrogen bonds are formed: semicarbazide to Tyr18, Arg108 and Val182 and nitrogen (pyridine) of the pyrazol-pyridine ring to Glu109. In contrast, compound **10c** formed one more hydrogen bond between semicarbazide and Glu109, which might interpret why compound **10c** has stronger *in vitro* activity. These interactions, especially interaction with semicarbazide, were identified as the crucial driving force for the S1PR2 binding. Furthermore, the pyrazol-pyridine ring, the isopropyl in **JTE-013** and the phenyl in **10c** occupied the hydrophobic channel, formed by six residues Ala36, Ile40, Phe86, Thr278, Phe274, and Ala275. Especially, one more hydrogen bond between **10c** and S1PR2 might be caused by the differences of hydrophobicity between isopropyl and phenyl, which leads to slight differences in the conformations of both molecules. In addition, the pyrrole-pyridine ring in **JTE-013** and **10c** could interact with the phenyl groups of Phe274 through π - π stacking. The other parts of the structures, dichloropyridine rings, also contributed to the interactions between S1PR2 and their inhibitors through the hydrophobicity of chlorine atoms.

JTE-013 and compound 10c reversed 5-FU resistance in HCT116^{DPD} cell xenograft model. To compare the anti-5-FU resistance properties of compounds **10c** and **JTE-013** *in vivo*, HCT116 cells with high DPD (HCT116^{DPD}) xenografted athymic mice model was established. In this model, we treated the mice with 20 mg/kg 5-FU combined with 1 mg/kg compound **10c** or 1 mg/kg **JTE-013** by tail vein injection for consecutive 24 days. As shown in Fig. 4A, body weights of 5-FU+**JTE-013**-treated mice rose again after the fall, whereas body weights of control groups and 5-FU+**10c** group continuously leveled off. Tumor growth was strongly inhibited by **JTE-013** plus 5-FU. The inhibition rate was greatly increased from 13.01% by single use of 5-FU to 75.87% by **JTE-013** plus 5-FU. In contrast, anti-5-FU resistance activity of compound **10c** was not as potent as **JTE-013** and the inhibition rate of compound **10c** plus 5-FU was 46.52% in HCT116^{DPD} xenografted athymic mice (Fig. 4B-D). In addition, JTE-013 monotherapy hardly affected the tumor proliferation with the inhibition rate of 3.41% in the HCT116^{DPD} model (Fig. S2).

To determine the activity of compounds **10c** and **JTE-013** in preventing DPD expression *in vivo*, we analyzed DPD levels in colons, tumors and livers of mice bearing HCT116^{DPD} xenograft. Western blotting assay showed that DPD was highly expressed in the livers, moderately expressed in the tumors and weakly expressed in normal colons (Fig. 5A). Compounds **10c** and **JTE-013** strongly inhibited DPD expression in both colonic tumors and livers (Fig. 5B). Immunohistochemistry with

DPD was also examined in the paraffin embedded tumor sections. As compared to the positive staining in a majority of tumoral, colonic and liver cells in control and 5-FU group, compounds **10c** and **JTE-013** strongly prevented DPD expressions (Fig. 5C).

As for 5-FU-induced S1PR2 internalization, tumoral tissues were all stained with S1PR2 by both immunohistochemical and immunofluorescent assays. As shown in Fig. 5D, S1PR2 merged with the ER marker Calnexin in cancer cells of 5-FU-treated mice, while S1PR2 maintained membranous expression in naïve mice. In contrast, there was no significant 5-FU-induced S1PR2 internalization in tumoral tissues after the treatment of compounds **10c** and **JTE-013**. These results indicated that compounds **10c** and **JTE-013** inhibited DPD expression through restraining the 5-FU-induced S1PR2 internalization.

JTE-013 reversed 5-FU resistance by reducing DPD-catalyzed degradation of intracellular 5-FU. Now that **JTE-013** significantly reversed 5-FU resistance by decreasing DPD expression *in vivo*, we sought to verify the role of **JTE-013** among various cell lines. As shown in Fig. 6A, DPD expression demonstrated the tendency of dose-dependent **JTE-013** treatment in HCT116, SW620 and cccHEL-1 cells but not in NCM460, Huh7 and Hela cells. Then we determined the inhibition rates of dose gradient of 5-FU combined with 5, 10 and 20 μM **JTE-013** in HCT116 and cccHEL-1 cells. Higher concentrations of **JTE-013** more effectively elevated the sensitivity of 5-FU treatment in HCT116 and cccHEL-1 cells (Fig. 6B). Since CDHP was taken as the

inhibitor of liver DPD [28], we subsequently compared the intracellular 5-FU levels between cccHEL-1 cells and HCT116 cells exposed to 5-FU (25 mg/L) which were respectively combined with CDHP (9 mg/L) or **JTE-013** (25 mg/L) for 6 h.

Impressively, on the one hand, HPLC-UV assay showed that the degradation of intracellular 5-FU was inhibited by both CDHP and **JTE-013** in cccHEL-1 cells. It showed that the concentration of intracellular 5-FU was only 0.068 mg/L in cccHEL-1 cells, while CDHP and **JTE-013** could increase the intracellular 5-FU to 14.003 mg/L and 16.769 mg/L, respectively (Fig. 6C and Fig. S3A-S3C). On the other hand, the degradation of intracellular 5-FU was only inhibited by **JTE-013** but not CDHP in HCT116 cells. It was determined that the intracellular 5-FU was 0.336 mg/L in HCT116 cells. CDHP did not significantly elevate the intracellular 5-FU, but **JTE-013** could increase the intracellular 5-FU to 5.763 mg/L (Fig. 6C and Fig. S3D-S3F). The tendency of corresponding FBAL levels was in accordance with the degradation of intracellular 5-FU (Fig. 6C). In addition, even though it was reported that **JTE-013** was designed as the inhibitor of S1PR2 [29], we also treated HCT116^{shS1PR2} and cccHEL-1^{shS1PR2} cells with 20 μ M **JTE-013** combined with dose gradient of 5-FU for further analyzing their inhibition rates. It depicts that **JTE-013** had no anti-5-FU resistance activity in the above HCT116^{shS1PR2} and cccHEL-1^{shS1PR2} cells, as compared to HCT116^{vector} and cccHEL-1^{vector} control cells (Fig. 6D). It thus further suggested the anti-5-FU resistance activity of **JTE-013** was due to targeting at S1PR2 but not through other targets. Overall, these results manifested that **JTE-013** reversed 5-FU

resistance by inhibiting DPD expression, which blocked the degradation of intracellular 5-FU into inactive FBAL in both liver and tumoral cells.

Discussion

This study was designed to develop a novel therapeutic strategy for overcoming 5-FU resistance. The major findings are as follows. First, our results demonstrate that S1PR2 is closely associated with the expression of DPD in various cancer cells. Second, by use of the S1PR2 inhibitor JTE-013 as molecular template, lead optimization was carried out in an attempt to improve potency and drug-like molecular properties by modifications of pyrroprymidine structure of JTE-013. In particular, successful conversion of the isopropyl and methyl moiety of JTE-013 into a phenyl and hydrogen moiety without loss of agonist potency led to a highly potent compound **10c**, which acted as the lowest EC₅₀ *in vitro*. Compound **10c** appears to be a promising agent that merits further investigation. In addition, *in silico* homology-docking suggested that Tyr18, Arg108 and Val182 and Glu109 may be critical residues to interact with antagonists, which contribute to a better understanding of pharmacological behaviors caused by the interaction with S1PR2. Third, compound **10c** exhibited weaker activity to reverse 5-FU resistance as compared with JTE-013 in mouse xenograft model, limiting its further investigation. We speculate that it may result from differences of metabolic stability. Para-hydrogen atom in the lipophilic phenyl ring is easily oxidized into 4-hydroxyl product by P450 enzyme in the liver,

which was rapidly metabolized. Overall, this study demonstrated that the promising compound, **JTE-013**, exhibited excellent inhibition on 5-FU resistance through suppressing DPD expression both *in vitro* and *in vivo*. Based on the above results, **JTE-013** has been selected as a lead candidate and is currently undergoing further characterization of the preclinical profile in our follow-up studies. In order to find better compounds to reverse 5-FU resistance, we will also further modify the leading compound to improve pharmacodynamics and pharmacokinetic properties of compound **10c**.

In summary, the present study identified S1PR2 as a potential upstream regulator of DPD expression, developed an approach to quickly obtain potent S1PR2 inhibitors and envisioned that an aromatic ring replacement would be suitable. In addition, we found a lead compound **10c** with good activity *in vitro* and a promising drug candidate **JTE-013** with excellent *in vivo* activity for further optimization and study.

Materials and Methods

Human cells lines. Human colorectal cancer cell lines HCT116 (ATCC[®] CCL-247TM), SW620 (ATCC[®] CCL-227TM), HT-29 (ATCC[®] HTB-38TM) and LOVO (ATCC[®] CCL-229). Human breast cancer cell line MCF-7 (MCF7 ATCC[®] HTB-22TM), human breast cancer cell line BT-474 (ATCC[®] HTB-20), cervical cancer cell line HeLa (ATCC[®] CCL-2) and hepatocellular cancer cell line Huh7 (ATCC[®] PTA-4583). Human liver healthy cell line cccHEL-1 and human colon healthy cell line

NCM460 (Incell Corp, San Antonio) were purchased from Shanghai Cell Bank, Chinese Academy of Science (Shanghai, China). Cells were maintained in RPMI-1640 or DMEM (Gibco) supplemented with 10% FBS (Gibco) at 37°C with 5% CO₂.

Stable transfection of shS1PR2 in cell lines. HCT116, SW620, Huh7 and cccHEL-1 cells were seeded in the 6-well plates containing 2 mL medium with cell density of 40-60% in each well. Remove media from wells and then add 2 mL media containing polybrene (final concentration 5 µg/ml) to each well. Gently swirl the plate to mix and remove the media containing lentiviral particles from wells. Fresh culture was substituted after 48 h and then 500 µg/ml of puromycin was added to the culture. After 7 to 10 days, the growth of puromycin-resistant cells was observed and selected clones were further grown in the medium containing 200 µg/ml of puromycin for 4 weeks. Puromycin-resistant clones named shS1PR2 cells were further propagated in the medium containing 10% FBS in the absence of puromycin and determined for S1PR2 expression by Western blotting assay. The transfection efficiency was affirmed by fluorescence microscopy. The Scramble_shRNA of the lentivirus is LV-U6>Scramble-shRNA-PGK>EGFP/Puro. The control sequence is CCTAAGGTTAAGTCGCCCTCG and the target sequence of S1PR2 is AGGAACAGCAAGTTCTACTCA.

TCGA dataset. RNA-seq data for individual TCGA cancer types were processed with a modified version of CrossHub, a tool for the multi-way analysis of TCGA transcriptomic and genomic data. Then they were normalized by TMM (the trimmed mean of M values) method and recalculated for 1 million library size. The derived TPM (transcripts per million) values were used to measure mRNA level of a gene for further analysis of expression stability. Gene expression values were transformed as $X' = \log_2(X + 1)$, where X represents the normalized fragments per kilobase transcript per million mapped reads values.

Subcutaneous tumor implantation in nude mice. Nude mice were caged under controlled temperature, humidity and light, fed with standard mouse chow. Under standard sterile conditions in the operating room, the xenografts of HCT116^{DPD} were established by inoculating 5×10^6 cells subcutaneously in mice. When the tumor reached a volume of 80-120 mm³, the mice were divided into four groups (n = 6) and administered by tail vein injection for consecutive 24 days. 5-FU, compounds 10c and JTE-013 were injected at doses of 20 mg/kg, 1 mg/kg and 1 mg/kg, respectively (dissolved in 30% PEG300, 5% Tween 80, 2% DMSO). Tumor volumes were assessed by bilateral Vernier caliper measurement every 4 days and calculated according to the following equation: [tumor volume = $X \times (Y^2/2)$], where X represents the longer and Y represents the shorter of the two dimensions. Body weight was also measured every 4 days, and clinical symptoms were observed daily. The

animals were sacrificed on day 24, and the tumors were removed and frozen in liquid nitrogen or fixed in 10% neutral-buffered formalin. The assays of western blotting, immunohistochemical and immunofluorescent staining were performed to test the proteins related to S1PR2 and DPD. All experiments in mice were approved by Animal Welfare Committee of Capital Medical University (permit no. AEEI-2016-043), in accordance with the animal care and use guidelines.

Quantitative RT-PCR. Total RNA was isolated by using Rneasy Mini Kit (74106, Qiagen). For cDNA synthesis, total RNA was transcribed by using PrimeScript (DRR047A, Takara, China). The levels of specific RNAs were measured by using ABI 7900 real-time PCR machine and Fast SybrGreen PCR mastermix according to the manufacturer's instructions. All samples, including the template controls, were assayed in triplicate. The relative number of target transcripts was normalized to GAPDH expression in the same sample. The relative quantification of target gene expression was performed with the standard curve or comparative cycle threshold (CT) method. Fold-induction was calculated by using the CT method as follows:

$$\Delta\Delta CT = (CT_{\text{target gene}} - CT_{\text{housekeeping gene}})_{\text{treatment}} - (CT_{\text{target gene}} - CT_{\text{housekeeping gene}})_{\text{nontreatment}}$$

Forward (5'-3') primer of *dpyd* is CCATCGCCATCGAGAGACAAG, and reward (5'-3') primer of *dpyd* is CACGTAGTGCTTAGCATAGAGAG. Forward (5'-3') primer of *Gapdh* is ACTCCAAGGCCACTTATCACC, and reward (5'-3') primer of *Gapdh* is ATTGTTACCAACTGGGACGAA.

Immunohistochemistry. Following de-paraffinization in xylene and rehydration, the slides were subject to high pH antigen retrieval (10 mmol/L citrate buffer; pH 9.0), followed by 3% hydrogen peroxide, and blocking in 1.5% serum. Slides were then incubated with the selected antibody at 4°C overnight. The information of primary antibodies is presented in Table S1. The slides were developed with an EnVision™ method (DAKO, Carpinteria, CA), visualized using diaminobenzidine solution, and then lightly counterstained with hematoxylin (H9627, Sigma). The IHC imaging was scanned by KF-PRO-OO5 slide viewer. Additionally, some slides were incubated with IgG1 isotype controls.

Western blotting analysis. Proteins were extracted by using RIPA Lysis Buffer (P0013, Beyotime, China) and quantified by using a BCA kit (P0009, Beyotime, China). Twenty micrograms of each protein sample were separated by 8, 10 or 15% SDS-PAGE and transferred to a polyvinylidene difluoride membrane. The membranes were blocked with 5% BSA and incubated with primary antibodies for 10 h at 4°C. The membranes were rinsed five times with PBS containing 0.1% Tween 20 and incubated for 1 h with appropriate horseradish peroxidase-conjugated secondary antibody at 37°C. Membranes were extensively washed with PBS containing 0.1% Tween 20 for three times. The signals were stimulated with enhanced chemiluminescence substrate (NEL105001 EA, PerkinElmer) for 1 min and detected

with a Bio-Rad ChemiDoc MP System (170-8280). The information of primary antibodies is presented in Table S1. The primary images (Fig. S4) were cropped for presentation.

MTT assay. Cell viability was assessed employing *in vitro* Toxicology Assay Kit-MTT Based, Stock No.TOX-1, Sigma. The key component is 3-[4,5-dimethylthiazol-2-yl]-2,5-diphenyl tetrazolium bromide (MTT). Cells paused at the logarithmic growth phase were inoculated into the 96-well plates at a concentration of 3×10^3 cells/ml. The cells of control group were incubated with 20 μ M 5-FU and tested compounds. The final concentrations of tested compounds were 0, 2.5, 5, 10, 20, 40, and 80 μ M, respectively. Each cell mass with final concentration were set into three holes. Each hole was routinely cultured for 48 h, and then added into 5 g/L \times 20 μ L MTT solution to incubate for 4 h. The supernatant in each hole was abandoned, and each hole was added with 150 μ L DMSO. After agitation for 5-10 min, the plates were sent to enzyme-labelled meter, and the A490 was detected at the 490 nm wave. The growth inhibition rate of each group was calculated as follows: Inhibition rate = $1 - (\text{OD}_{\text{Drug}} - \text{OD}_{\text{Blank}}) / (\text{OD}_{\text{Control}} - \text{OD}_{\text{Blank}})$. The values of EC50 (tested compound plus 20 μ M 5-FU) and IC50 (tested compound only) were determined according to their growth inhibition rates.

Immunofluorescent assay. CRC cells (2.5×10^4) were seeded onto the 12-mm glass coverslips in 6-well plates. Cells were fixed in 4.5% paraformaldehyde for 15 min, washed in PBS, permeabilized with 1×Perm/Wash Buffer (BD Biosciences) for 10 min, washed in PBS, blocked for nonspecific antibody reactions by incubating in the solution containing 5% BSA for 30 min, and incubated with anti-Calnexin or anti-S1PR2 antibodies. Secondary antibodies included donkey anti-rabbit IgG (Alexa Fluor® 488, Invitrogen) and labeled goat anti-mouse IgG (Alexa Fluor® 648, CST). Coverslips were mounted with Vectashield® antifade mounting medium containing DAPI (Sigma-Aldrich). Confocal laser microscopy was performed on a Leica TCS SP5 AOBS apparatus, using excitation spectral laser lines at 488 nm. Image acquisition and processing were conducted using Leica Confocal Software (Leica Microsystems).

HPLC analysis of intracellular 5-FU and FBAL. 5-FU and FBAL ranged from 0.2 to 50 mg/L for preparation of the standard curves. Cells were inoculated in 6-well plate and then treated with 5-FU (25 mg/L) for 6 h. After cell counting, cells were resuspended in 150 µl PBS and lysed by sonication in ice-water bath for 30 min. The procedure of solid-phase extraction was utilized with styrene-divinylbenzene resin SPE columns as shown before [30]. Then the samples were centrifuged at 10,000 g for 15 min. The fresh supernatants were filtered and injected into HPLC (Waters

QDA) for analysis. The concentrations of 5-FU and FBAL were calculated from the respective calibration curves.

Molecular Docking. The structures of compounds **10c** and **JTE-013** were built using ChemDraw14.0, followed by MM2 energy minimization. The molecular docking study was performed using LeDock Tools in combination with PyMOL software. The homology model of S1PR2 based on the high-resolution crystal structure of the S1PR1 (PDB: 3V2Y) was used for the docking studies performed here. The interaction of protein and ligands in the binding pocket was defined in LeDock. Each docking experiment was performed 20 times, yielding 20 docked conformations. All of other parameters used in the docking process were the default values of the system. The best binding modes were picked based on the best stabilization energy.

Statistical analysis

Statistical analysis was conducted by GraphPad Prism 5. After checking data for normal distribution and variance homogeneity, continuous data were compared using the Mann-Whitney U test, multiple Student t tests or two-way ANOVA. All p values are two-tailed, and p values < 0.05 were considered significant ($*p < 0.05$, $**p < 0.01$ and $***p < 0.001$). The data are represented as mean \pm S.E.M. or the median with 10 and 90 percentiles. All statistical tests were two-sided.

Author's contribution

Xian-Jun Qu and Sheng-Biao Wan conceived and designed the study. Yu-Hang Zhang performed animals and cellular studies experiments. Dong-Dong Luo designed, synthesized and analyzed all of the compounds. Yu-Hang Zhang and Dong-Dong Luo wrote the manuscript, which was edited by all authors.

Conflict of interest: The authors declare no potential conflicts of interest.

Acknowledgements: This work was supported by National Natural Science Foundation of China (91629303/81673449/81872884/81973350) and Beijing Natural Science Foundation and Scientific Research Program of Municipal Commission of Education (KZ201710025020/KZ201810025033).

References:

- [1] B. Gustavsson, G. Carlsson, D. Machover, N. Petrelli, A. Roth, H.J. Schmoll, K.M. Tveit, F. Gibson, A review of the evolution of systemic chemotherapy in the management of colorectal cancer, *Clin Colorectal Cancer* 14 (2015) 1-10.
- [2] J.A. Meyerhardt, R.J. Mayer, Systemic therapy for colorectal cancer, *N Engl J Med* 352 (2005) 476-487.
- [3] P. Noordhuis, U. Holwerda, C.L. Van der Wilt, C.J. Van Groeningen, K. Smid, S. Meijer, H.M. Pinedo, G.J. Peters, 5-Fluorouracil incorporation into RNA and DNA in relation to thymidylate synthase inhibition of human colorectal cancers, *Ann Oncol* 15 (2004) 1025-1032.
- [4] D.B. Longley, D.P. Harkin, P.G. Johnston, 5-fluorouracil: mechanisms of action and clinical strategies, *Nat Rev Cancer* 3 (2003) 330-338.
- [5] F. Innocenti, R. Danesi, G. Bocci, G. Natale, T.M. Del, 5-Fluorouracil catabolism to 5-fluoro-5,6-dihydrouracil is reduced by acute liver impairment in mice, *Toxicol Appl Pharmacol* 203 (2005) 106-113.
- [6] R.B. Diasio, B.E. Harris, Clinical pharmacology of 5-fluorouracil, *Clin Pharmacokinet* 16 (1989) 215-237.
- [7] M. Kornmann, W. Schwabe, S. Sander, M. Kron, J. Strater, S. Polat, E. Kettner, H.F. Weiser, W. Baumann, H. Schramm, P. Hausler, K. Ott, D. Behnke, L. Staib, H.G. Beger, K.H. Link, Thymidylate synthase and dihydropyrimidine dehydrogenase

mRNA expression levels: predictors for survival in colorectal cancer patients

receiving adjuvant 5-fluorouracil, *Clin Cancer Res* 9 (2003) 4116-4124.

[8] A.M. Lee, Q. Shi, S.R. Alberts, D.J. Sargent, F.A. Sinicrope, J.L. Berenberg, A.

Grothey, B. Polite, E. Chan, S. Gill, M.S. Kahlenberg, S.G. Nair, A.F. Shields, R.M.

Goldberg, R.B. Diasio, Association between DPYD c.1129-5923 C>G/hapB3 and

severe toxicity to 5-fluorouracil-based chemotherapy in stage III colon cancer

patients: NCCTG N0147 (Alliance), *Pharmacogenet Genomics* 26 (2016) 133-137.

[9] D. Rosmarin, C. Palles, A. Pagnamenta, K. Kaur, G. Pita, M. Martin, E.

Domingo, A. Jones, K. Howarth, L. Freeman-Mills, E. Johnstone, H. Wang, S. Love,

C. Scudder, P. Julier, C. Fernandez-Rozadilla, C. Ruiz-Ponte, A. Carracedo, S.

Castellvi-Bel, A. Castells, A. Gonzalez-Neira, J. Taylor, R. Kerr, D. Kerr, I.

Tomlinson, A candidate gene study of capecitabine-related toxicity in colorectal

cancer identifies new toxicity variants at DPYD and a putative role for ENOSF1

rather than TYMS, *Gut* 64 (2015) 111-120.

[10] K.E. Caudle, C.F. Thorn, T.E. Klein, J.J. Swen, H.L. McLeod, R.B. Diasio, M.

Schwab, Clinical Pharmacogenetics Implementation Consortium guidelines for

dihydropyrimidine dehydrogenase genotype and fluoropyrimidine dosing, *Clin*

Pharmacol Ther 94 (2013) 640-645.

[11] W.H. Gmeiner, Novel chemical strategies for thymidylate synthase inhibition,

Curr Med Chem 12 (2005) 191-202.

- [12]G.J. Peters, C.L. van der Wilt, C.J. van Groeningen, K. Smid, S. Meijer, H.M. Pinedo, Thymidylate synthase inhibition after administration of fluorouracil with or without leucovorin in colon cancer patients: implications for treatment with fluorouracil, *J Clin Oncol* 12 (1994) 2035-2042.
- [13]K. Tatsumi, M. Fukushima, T. Shirasaka, S. Fujii, Inhibitory effects of pyrimidine, barbituric acid and pyridine derivatives on 5-fluorouracil degradation in rat liver extracts, *Jpn J Cancer Res* 78 (1987) 748-755.
- [14]K. Hirata, N. Horikoshi, K. Aiba, M. Okazaki, R. Denno, K. Sasaki, Y. Nakano, H. Ishizuka, Y. Yamada, S. Uno, T. Taguchi, T. Shirasaka, Pharmacokinetic study of S-1, a novel oral fluorouracil antitumor drug, *Clin Cancer Res* 5 (1999) 2000-2005.
- [15]M. Nakamura, H. Nagano, S. Marubashi, A. Miyamoto, Y. Takeda, S. Kobayashi, H. Wada, T. Noda, K. Dono, K. Umeshita, M. Monden, Pilot study of combination chemotherapy of S-1, a novel oral DPD inhibitor, and interferon-alpha for advanced hepatocellular carcinoma with extrahepatic metastasis, *Cancer-Am Cancer Soc* 112 (2008) 1765-1771.
- [16]R. Wu, Q. Nie, E.E. Tapper, C.R. Jerde, G.S. Dunlap, S. Shrestha, T.A. Elraiyah, S.M. Offer, R.B. Diasio, Histone H3K27 Trimethylation Modulates 5-Fluorouracil Resistance by Inhibiting PU.1 Binding to the DPYD Promoter, *Cancer Res* 76 (2016) 6362-6373.

- [17] A. Vestri, F. Pierucci, A. Frati, L. Monaco, E. Meacci, Sphingosine 1-Phosphate Receptors: Do They Have a Therapeutic Potential in Cardiac Fibrosis? *Front Pharmacol* 8 (2017) 296.
- [18] L. Kappos, J. Antel, G. Comi, X. Montalban, P. O'Connor, C.H. Polman, T. Haas, A.A. Korn, G. Karlsson, E.W. Radue, Oral fingolimod (FTY720) for relapsing multiple sclerosis, *N Engl J Med* 355 (2006) 1124-1140.
- [19] J.A. Cohen, F. Barkhof, G. Comi, H.P. Hartung, B.O. Khatri, X. Montalban, J. Pelletier, R. Capra, P. Gallo, G. Izquierdo, K. Tiel-Wilck, A. de Vera, J. Jin, T. Stites, S. Wu, S. Aradhye, L. Kappos, Oral fingolimod or intramuscular interferon for relapsing multiple sclerosis, *N Engl J Med* 362 (2010) 402-415.
- [20] S.P. Cramer, H.J. Simonsen, A. Varatharaj, I. Galea, J.L. Frederiksen, H. Larsson, Permeability of the blood-brain barrier predicts no evidence of disease activity at 2 years after natalizumab or fingolimod treatment in relapsing-remitting multiple sclerosis, *Ann Neurol* 83 (2018) 902-914.
- [21] N.C. Hait, L.E. Wise, J.C. Allegood, M. O'Brien, D. Avni, T.M. Reeves, P.E. Knapp, J. Lu, C. Luo, M.F. Miles, S. Milstien, A.H. Lichtman, S. Spiegel, Active, phosphorylated fingolimod inhibits histone deacetylases and facilitates fear extinction memory, *Nat Neurosci* 17 (2014) 971-980.
- [22] B. Zemann, B. Kinzel, M. Muller, R. Reuschel, D. Mechtcheriakova, N. Urtz, F. Bornancin, T. Baumruker, A. Billich, Sphingosine kinase type 2 is essential for

lymphopenia induced by the immunomodulatory drug FTY720, *Blood* 107 (2006)

1454-1458.

[23] J.A. Cohen, J. Chun, Mechanisms of fingolimod's efficacy and adverse effects in multiple sclerosis, *Ann Neurol* 69 (2011) 759-777.

[24] V. Rothhammer, J.E. Kenison, E. Tjon, M.C. Takenaka, K.A. de Lima, D.M.

Borucki, C.C. Chao, A. Wilz, M. Blain, L. Healy, J. Antel, F.J. Quintana, Sphingosine 1-phosphate receptor modulation suppresses pathogenic astrocyte activation and chronic progressive CNS inflammation, *Proc Natl Acad Sci U S A* 114 (2017) 2012-2017.

[25] L. Zhang, H.D. Wang, X.J. Ji, Z.X. Cong, J.H. Zhu, Y. Zhou, FTY720 for cancer therapy (Review), *Oncol Rep* 30 (2013) 2571-2578.

[26] L. Pouzol, L. Piali, C.C. Bernard, M.M. Martinic, B. Steiner, M. Clozel,

Therapeutic Potential of Ponesimod Alone and in Combination with Dimethyl

Fumarate in Experimental Models of Multiple Sclerosis, *Innov Clin Neurosci* 16

(2019) 22-30.

[27] L. Peyrin-Biroulet, R. Christopher, D. Behan, C. Lassen, Modulation of

sphingosine-1-phosphate in inflammatory bowel disease, *Autoimmun Rev* 16 (2017)

495-503.

[28] M.W. Saif, L.S. Rosen, K. Saito, C. Zergebel, L. Ravage-Mass, D.S. Mendelson,

A phase I study evaluating the effect of CDHP as a component of S-1 on the

pharmacokinetics of 5-fluorouracil, *Anticancer Res* 31 (2011) 625-632.

[29]N.J. Pyne, S. Pyne, Selectivity and specificity of sphingosine 1-phosphate receptor ligands: "off-targets" or complex pharmacology? *Front Pharmacol* 2 (2011)

26.

[30]G. Micoli, R. Turci, M. Arpellini, C. Minoia, Determination of 5-fluorouracil in environmental samples by solid-phase extraction and high-performance liquid chromatography with ultraviolet detection, *J Chromatogr B Biomed Sci Appl* 750 (2001) 25-32.

Journal Pre-proof

Figure legends

Figure 1. Identification of S1PR2 as the potential upstream regulator of DPYD expression in TCGA database and cell lines. (A) The profiles of S1PR2 expression in a variety of tumor types and paracancerous tissues in TCGA datasets. The heights of the bars represent the transcripts per million (TPM) of tumoral samples and paracancerous tissues. The abbreviations of tumors in TCGA database are listed in Table S2. (B) The comparison of S1PR2 expression levels between tumoral and paracancerous tissues in colorectal adenocarcinoma (COAD), skin cutaneous melanoma (SKCM) and rectum adenocarcinoma (READ). The differences in S1PR2 levels between tumoral and paracancerous tissues in these cancer types were more significant than other cancer types. $\text{Log}_2(\text{TPM} + 1)$ was used for log-scale. Calculated means \pm SEM were represented by bars and whiskers. (C) The correlations of S1PR2 to DPYD (left), TYMS (middle) and TYMP (right) were presented in colorectal cancer tissues. The correlation coefficient R values of S1PR2 to DPYD, TYMS and TYMP were 0.75, -0.4, 0.35, respectively. (D) The correlations of S1PR2 to DPYD (left), TYMS (middle) and TYMP (right) in paracancerous tissues. The correlation coefficient R values of S1PR2 to DPYD, TYMS and TYMP were 0.31, 0.46, 0.19, respectively. (E) Western blotting analyzed the expression levels of S1PR2 and DPD in various naïve cell lines, including HCT116, HT-29, SW620, LOVO, NCM460, MCF-7, BT474, Hela, Huh7 and cccHEL-1 cells. A satisfying consistence was seen between the expressions of S1PR2 and DPD. (F) RT-qPCR assay analyzed the

expressions of S1PR2 and DPD in mRNA level among the above 10 cell lines, which was consistent with the tendency of protein levels. (G) HCT116, SW620, Huh7 and cccHEL-1 cells of transfecting with shS1PR2 demonstrated decreased DPD expression as compared with vector control cells. (H) Inhibition rates of 5-FU were detected by the MTT assay in HCT116, SW620, Huh7 and cccHEL-1 cells of transfecting with shS1PR2. Dose gradient of 5-FU treatment ranged from 0 to 100 μM . Data information: In (E, F and H), data are presented as mean \pm SEM. * $p < 0.05$, ** $p < 0.01$ and *** $p < 0.001$ (Student's t-test).

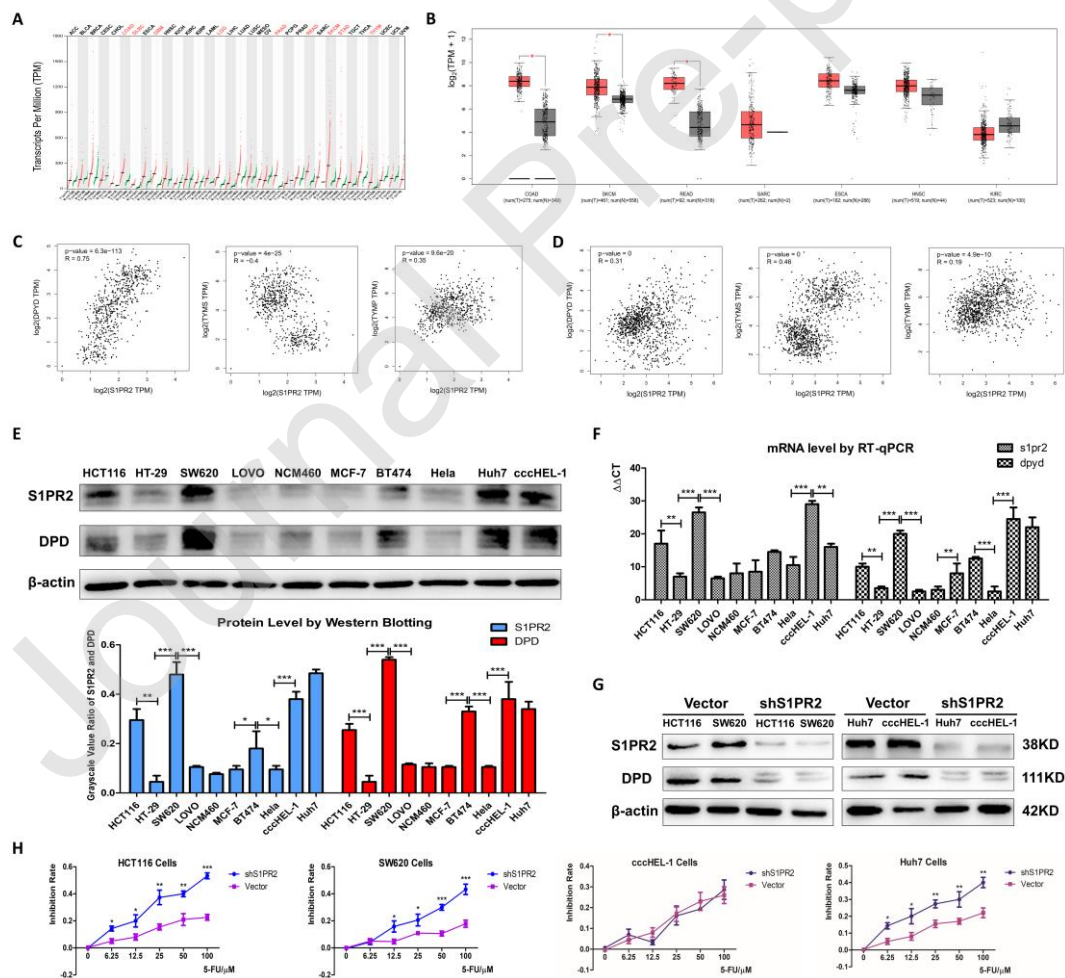


Figure 2. S1PR2 inhibitors suppressed DPD expression in cancer cells. (A) Treated with compounds **14a**, **14e**, **10c**, **18b** and **JTE-013**, the expressions of DPD, JMJD3 and H3K27me3 HCT116 cells were determined by western blotting assay. The ratios of their corresponding grayscale values to β -actin were statistically illuminated in the right panel. Data are presented as mean \pm SEM. * $p < 0.05$, ** $p < 0.01$ and *** $p < 0.001$ (Student's t-test). (B) Immunofluorescent assay determined S1PR2 internalization in HCT116 cells. S1PR2 (green) merged with the ER marker Calnexin (red) in the 5-FU-treated (10 μ M) HCT116 cells, while S1PR2 maintained membranous localization in naïve HCT116 cells. Compounds **10c** and **JTE-013** effectively prevented 5-FU-induced S1PR2 internalization (scale bar: 75 μ m).

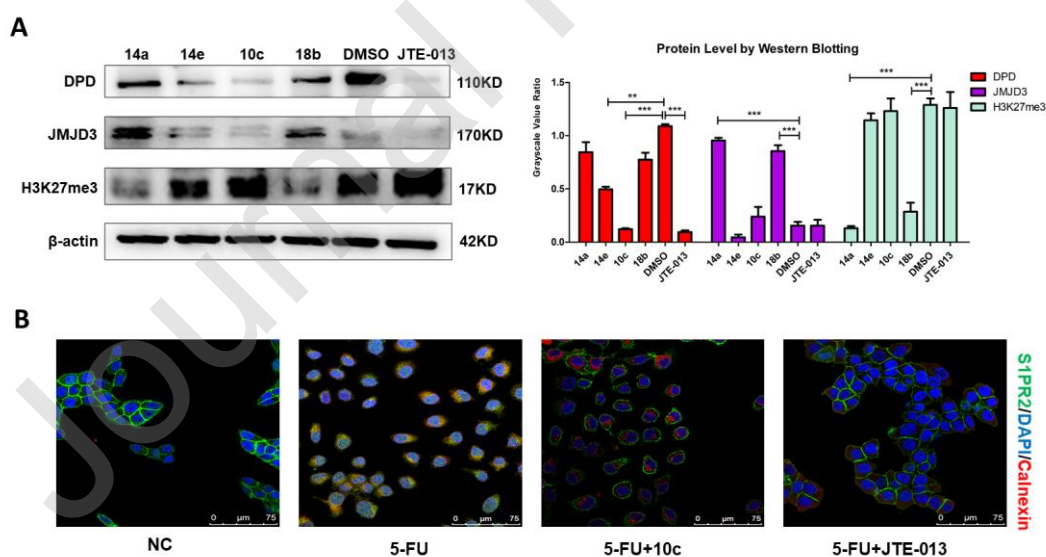


Figure 3. Molecular docking studies. (A) X-ray structure of S1PR1 (PDB ID: 3V2Y)

and the homology model of human S1PR2 with a schematic representation of the putative binding site deduced from S1PR1 crystal structure. (B) The chemical structure of **JTE-013** and compound **10c**. (C) Proposed binding mode of **JTE-013** (green carbon sticks) in a homology model (off-white ribbons) of S1PR2. (D) Proposed binding mode of compound **10c** (carmine carbon sticks) in a homology model (off-white ribbons) of S1PR2. Atom color code: red = oxygen, blue = nitrogen, white = hydrogen, yellow = sulfur, cyan = fluorine. Hydrogen bonds between the ligand and receptor are indicated by yellow dashed lines.

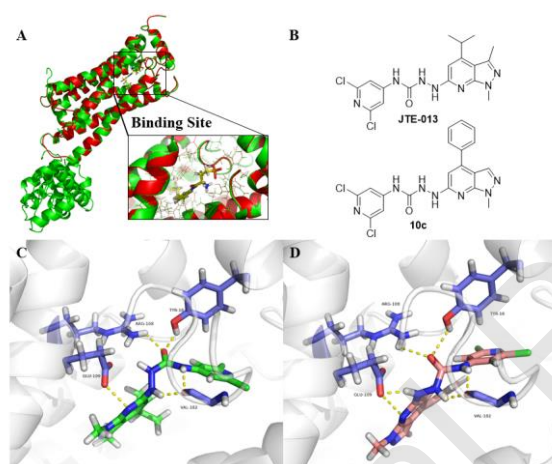


Figure 4. The inhibitory effects of compounds **10c** and **JTE-013** on 5-FU resistance in the HCT116^{DPD} xenografted athymic mice. Compounds **10c** and **JTE-013** dissolved in 30% PEG300, 5% Tween 80, 2% DMSO were daily administered by tail vein injection for consecutive 24 days. (A) Body weights of single 5-FU group, 5-FU combined with **JTE-013** group, 5-FU combined with compound **10c** group and solvent control group were measured every four days, n = 6. (B) Tumor volumes were recorded every four days and the inhibition rates were calculated based on the ratio of

ultimate tumor volume of each treatment group to the solvent group, $n = 6$. (C)

Representative tumor-bearing nude mice of each group, $n = 6$. (D) Removed tumors

of each group, $n = 6$. Data information: In (A, B), data are presented as mean \pm SEM.

* $p < 0.05$, ** $p < 0.01$ and *** $p < 0.001$ (Student's t-test).

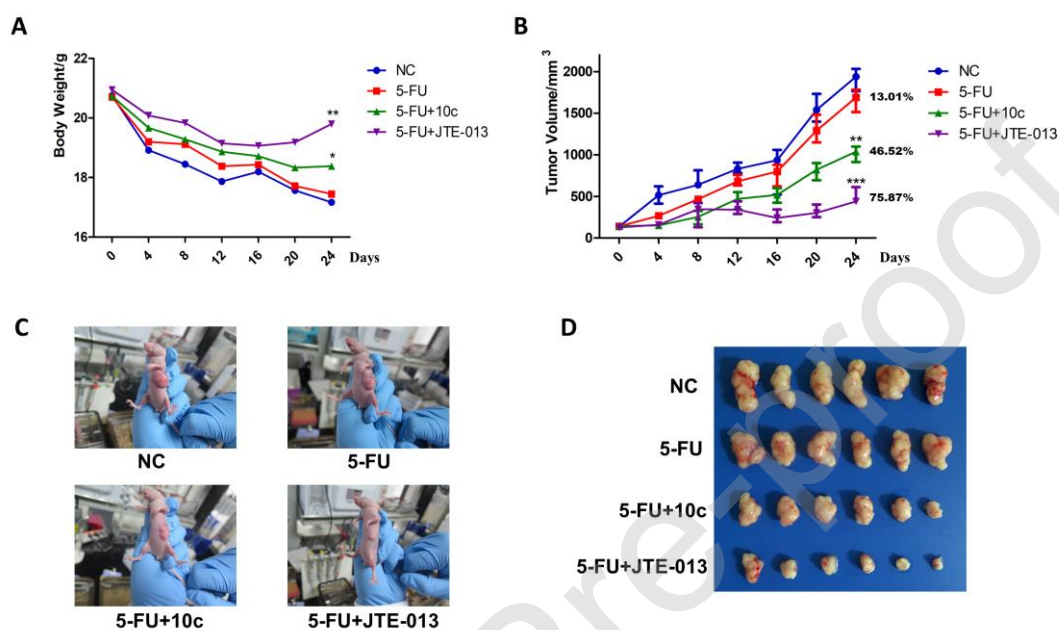


Figure 5. Compounds **10c** and **JTE-013** prevented 5-FU resistance *in vivo* by

downregulating DPD expression. (A) The comparison of DPD levels in liver, colon and tumoral tissues of naïve nude mice as assayed by western blotting analysis, $n = 4$.

(B) DPD expressions were analyzed in liver, colon and tumoral tissues of single 5-FU group, 5-FU combined with **JTE-013** group, 5-FU combined with compound **10c**

group and solvent control group, $n = 6$. (C) Detected by immunohistochemistry, DPD expressions were analyzed in liver, colon and tumoral tissues of each group, $n = 6$.

(D) Assayed by immunohistochemistry, S1PR2 internalization was determined in cancer cells of 5-FU treated nude mice, while compounds **10c** and **JTE-013**

suppressed 5-FU-induced internalization of S1PR2. Immunofluorescent analysis

Figure 6. JTE-013 reversed 5-FU resistance by reducing DPD-catalyzed degradation of intracellular 5-FU. (A) Treated with 5, 10 and 20 μ M JTE-013, DPD expressions were determined in various cell lines, including SW620, HCT116, NCM460, cccHEL-1, Huh7 and Hela cells. (B) Treated with 5, 10 and 20 μ M JTE-013, the inhibition rates of dose-gradient 5-FU were measured by the MTT assay in HCT116 and cccHEL-1 cells. (C) HPLC-UV/vis analyzed intracellular 5-FU and FBAL in cccHEL-1 cells and HCT116 cells treated with 5-FU (25 mg/L) combined with CDHP (9 mg/L) or **JTE-013** (25 mg/L) for 6 h. Ten microliters of sample were subjected to HPLC with a Spherisorb ODS-2 column which was eluted with methanol-water. Based on the standard curves of 5-FU and FBAL, the concentration of 5-FU and FBAL were statistically analyzed in the right histogram. (D) To exclude the effect of other targets for JTE-013, dose gradient of 5-FU was combined with 20 μ M JTE-013 to treat HCT116 and cccHEL-1 cells of transfecting with shS1PR2. Then the inhibition rates of 5-FU were measured by the MTT assay. Data information: In (A-D), data are presented as mean \pm SEM. * p < 0.05, ** p < 0.01 and *** p < 0.001 (Student's t-test).

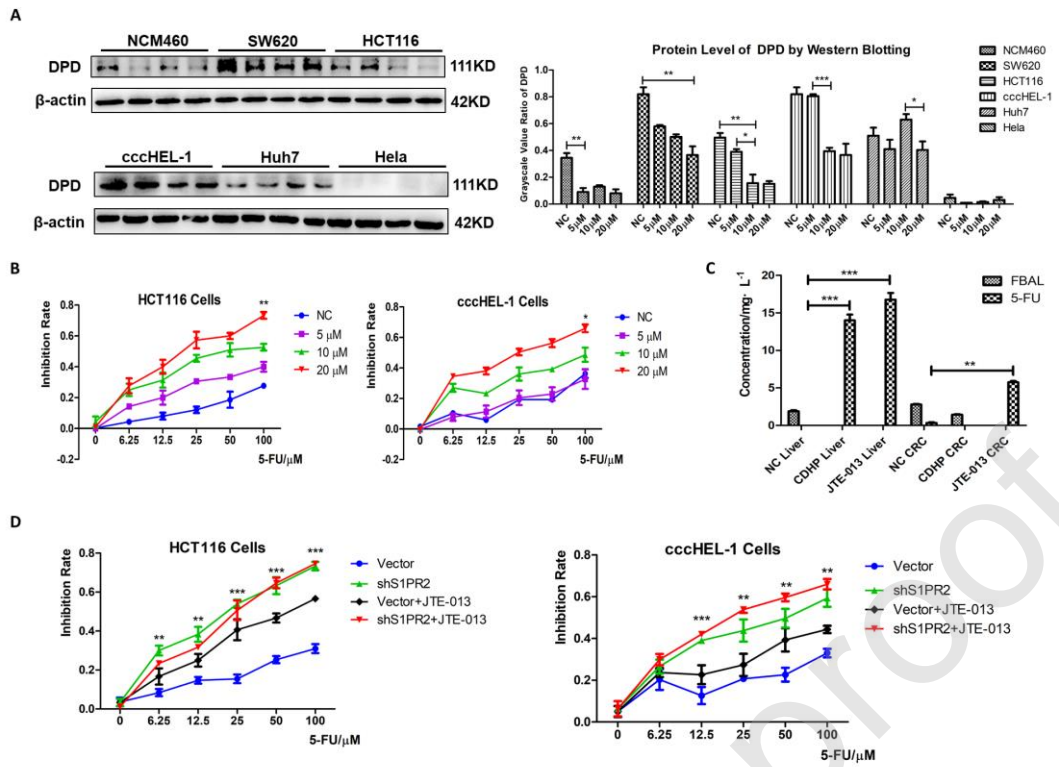
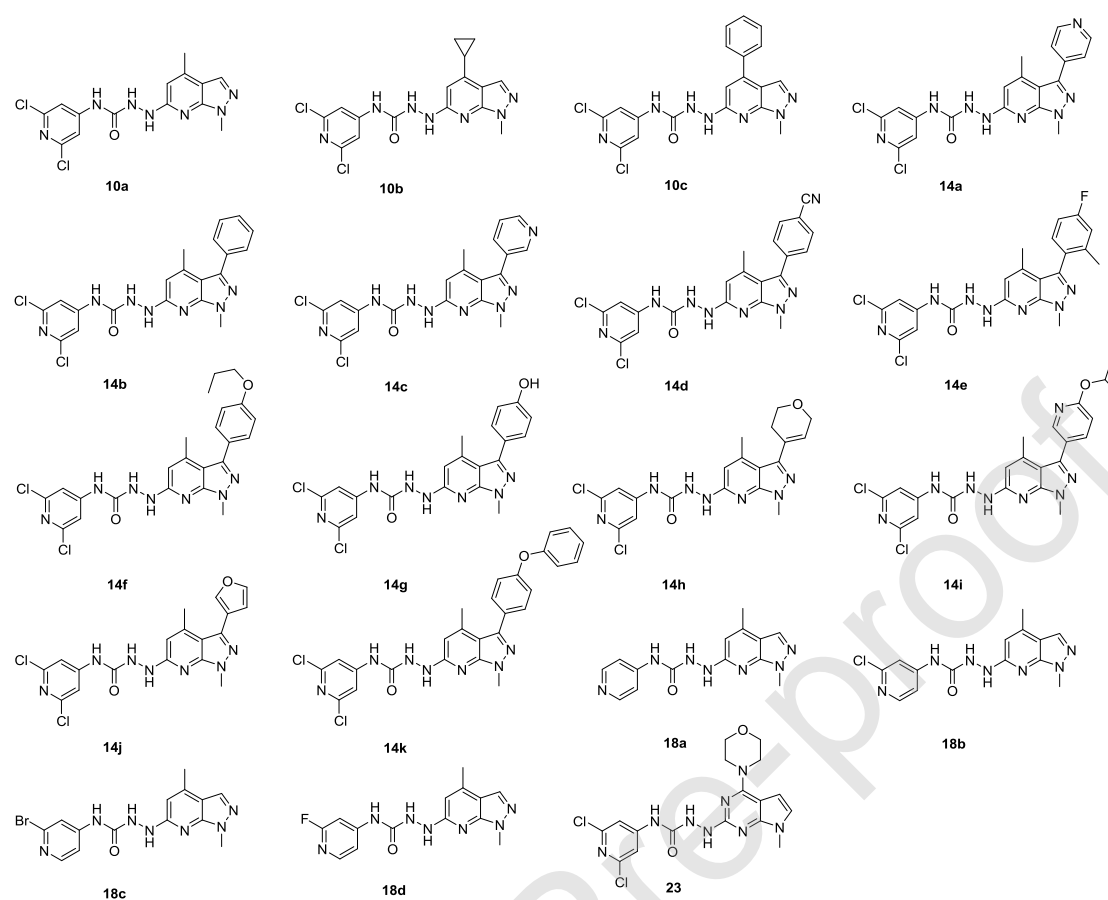


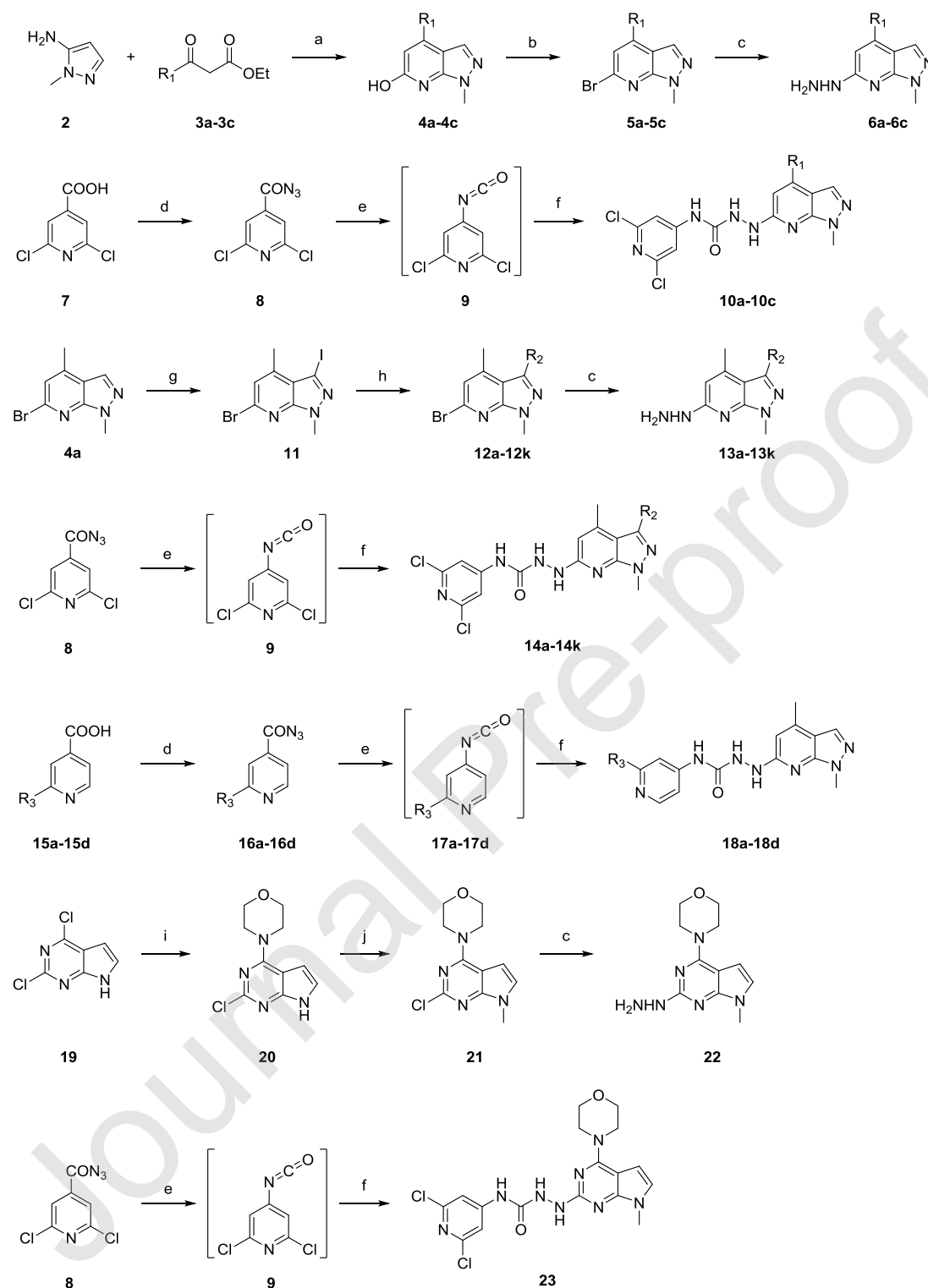
Table 1



Compd	IC ₅₀ (μM) ^a			EC ₅₀ (μM) ^a		
	HCT116	HT29	NCM460	HCT116	HT29	NCM460
JTE-013	57.13 ± 0.25	59.66 ± 1.01	68.56 ± 0.78	18.28 ± 1.46	57.13 ± 0.25	68.56 ± 0.78
10a	73.16 ± 0.93	87.45 ± 2.64	95.45 ± 6.41	47.25 ± 1.42	73.16 ± 0.93	95.45 ± 6.41
10b	75.36 ± 2.12	83.14 ± 1.56	89.25 ± 1.72	25.45 ± 0.23	75.36 ± 2.12	89.25 ± 1.72
10c	76.24 ± 2.92	79.91 ± 2.54	99.12 ± 4.22	6.24 ± 0.92	76.24 ± 2.92	99.12 ± 4.22
14a	57.63 ± 2.16	62.14 ± 2.01	83.12 ± 4.31	13.14 ± 1.43	57.63 ± 2.16	83.12 ± 4.31
14b	49.27 ± 0.74	58.68 ± 1.92	79.28 ± 1.67	36.27 ± 0.74	49.27 ± 0.74	79.28 ± 1.67
14c	66.12 ± 0.52	72.63 ± 1.43	83.23 ± 0.97	28.12 ± 0.52	66.12 ± 0.52	83.23 ± 0.97
14d	85.43 ± 0.41	83.17 ± 1.04	91.23 ± 3.25	35.11 ± 1.76	85.43 ± 0.41	91.23 ± 3.25

14e	33.26 ± 0.87	45.16 ± 1.21	59.27 ± 7.12	13.24 ± 1.56	33.26 ± 0.87	59.27 ± 7.12
14f	85.13 ± 1.46	95.46 ± 2.14	98.13 ± 0.65	31.25 ± 0.52	85.13 ± 1.46	98.13 ± 0.65
14g	55.35 ± 3.11	67.66 ± 2.11	89.01 ± 0.91	45.62 ± 7.82	55.35 ± 3.11	89.01 ± 0.91
14h	54.11 ± 5.46	55.21 ± 3.66	60.13 ± 2.14	33.25 ± 8.74	54.11 ± 5.46	60.13 ± 2.14
14i	5.21 ± 0.34	38.14 ± 2.23	146.34 ± 2.13	6.14 ± 1.72	5.21 ± 0.34	116.34 ± 2.13
14j	23.40 ± 1.54	34.33 ± 1.23	65.26 ± 0.89	55.24 ± 0.72	23.40 ± 1.54	65.26 ± 0.89
14k	41.50 ± 0.73	34.26 ± 0.57	77.53 ± 0.55	48.25 ± 1.57	41.50 ± 0.73	77.53 ± 0.55
18a	104.18 ± 0.65	132.16 ± 1.76	154.41 ± 0.73	63.21 ± 1.81	104.18 ± 0.65	154.41 ± 0.73
18b	76.13 ± 1.78	70.01 ± 0.59	85.74 ± 0.61	38.15 ± 1.37	76.13 ± 1.78	85.74 ± 0.61
18c	78.45 ± 0.84	75.46 ± 3.17	89.12 ± 3.45	39.28 ± 1.85	78.45 ± 0.84	89.12 ± 3.45
18d	89.23 ± 0.56	99.46 ± 0.57	81.12 ± 3.15	59.17 ± 1.12	89.23 ± 0.56	81.12 ± 3.15
23	63.12 ± 0.97	77.67 ± 2.13	93.43 ± 2.12	47.15 ± 1.43	63.12 ± 0.97	93.43 ± 2.12

^aIC₅₀ and EC₅₀ values were determined at least three separate experiments (n ≥ 3). The values are shown as mean with error in square brackets expressed as the 95% confidence interval. The EC₅₀ values were determined through combining with 20 μM 5-FU.

Scheme 1. Synthetic Route to S1PR2 inhibitors 10a–10c, 14a–14k, 18a–18d, 23^a

^aReagents and conditions: (a) acetic acid, 130 °C, 3-10 h, 15-60%; (b) POBr₃, anisole, reflux, 31-85%; (c) 80% hydrazine hydrate, EtOH, reflux, 90-95%; (d)

diphenylphosphoryl azide, Et₃N, 1,4-dioxane, 61-80%; (e) toluene, 80 °C; (f) THF, **6a-6c**, **13a-13k** or **22**, 50 °C, 35-59% over two steps. (g) NIS, 48% HBF₄, CH₃CN, 80 °C, 2 h, 76%; (h) boric acid or borate, PdCl₂ (dppf), CsF, 1,4-dioxane/H₂O, 80 °C, 30-55%; (i) morpholine, EtN₃, DCM, rt, overnight, 89%; (j) CH₃I, NaH, DMF, 0 °C, 90%.

Journal Pre-proof